Extreme dielectric non-linearities at the convergence point in Ba1-xCaxTi1-xZrxO3 thin films

Quentin Simon, Christophe Daumont, Sandrine Payan, P. Gardes, Patrick Poveda, Jérôme Wolfman, Mario Maglione

Extreme dielectric non-linearities at the convergence point in $Ba_{1-x}Ca_xTi_{1-x}Zr_xO_3$ thin films

Q. Simon[1,2], C. J. M. Daumont[2], S. Payan[1], P. Gardes[3], P. Poveda[3], J. Wolfman[2], M. Maglione[1]

1. Institut de Chimie de la Matière condensée de Bordeaux, UPR 9048 ICMCB-CNRS, Université de Bordeaux, 33608 Pessac Cedex, France

2. Laboratoire GREMAN, UMR7347 CNRS, Université de Tours, 37200 Tours, France

3. STMicroelectronics, 10 rue Thalès de Milet, 37071 Tours, France

Abstract

The dielectric properties of $Ba_{1-x}Ca_xTi_{1-x}Zr_xO_3$ (BCTZ) thin films are explored by varying x from 0 to 0.18 through an RF magnetron co-sputtering process. Thin films are analyzed by Rutherford Backscattering Spectroscopy, X-Ray Diffraction and dielectric measurements on parallel plate capacitors as a function of temperature (from 100 to 420K), frequency (from 100 Hz to 1 MHz) and static electric field (from 0 to 250 kV/cm). The evolutions of their dielectric properties with composition are systematically compared to bulk ceramic counterparts. In both cases, a continuous crossover from classical-to-relaxor ferroelectric behavior along with a decrease of the temperature of the permittivity maximum are observed as x increases. Besides, a phase convergence region (PCR) between cubic, tetragonal, orthorhombic and rhombohedral symmetries is evidenced for compositions close to x = 0.12. This is the first time that such a PCR is observed in thin films. At this point in the phase diagram, all of the dielectric parameters undergo specific variations. In particular, the enhanced permittivity dependence to external electric field for these Ca and Zr contents is attributed to an emerging relaxor behavior together with its vicinity of the PCR. These results make BCTZ thin films potential candidates to achieve electrically tunable devices.

Keywords: BCTZ; thin film; dielectric; tunable capacitors; sputtering; lead-free relaxor

1. Introduction

Ferroelectric oxide thin films endowed by high tunability (*ie* high non-linear variation of their dielectric permittivity ε' under an external electric field), low dielectric losses (tan δ) and low leakage current together with good thermal stability are attractive candidates to design miniaturized and electrically reconfigurable devices. The integration of ferroelectric-based tunable devices, such as capacitors, impedance matching systems, filters/resonators or phase shifters, enables to achieve wireless telecommunication platforms that can cover more and more functions while keeping low bulkiness and power consumption.[1–3]

Most of the researches are focused on derivative compounds from the archetypal ferroelectric $BaTiO_3$ (BT), whose spontaneous/induced polarization mainly arises from the shift of Ti^{4+} ions from the center of the BO_6 octahedral cage of the ABO_3 perovskite structure. Hence, BT ferroelectric properties strongly depend on its crystal symmetry, which varies from the high temperature cubic (C) paraelectric phase to the tetragonal (T), orthorhombic (O) and rhombohedral (R) ferroelectric phases as the temperature decreases. Besides, the polarizability dependencies to external stresses (such as pressure or electric field) are enhanced in the vicinity of the structural transitions.

The $BaTiO_3$-$CaTiO_3$-$BaZrO_3$ ternary system (BCTZ) attracts a great attention since the BT ferroelectric features can be tailored either with A- or B-site aliovalent substitutions in order to tune the dielectric properties and to bring structural transitions close to a targeted operating temperature. Bulk BCTZ ceramics show a complex structural phase diagram leading to rich varieties of dielectric features including classical ferroelectric, incipient ferroelectric, diffuse or relaxor behaviors.[4] Starting from BT, substitution with zirconium reduces the paraelectric-to-ferroelectric transition temperature as well as the number of structural transition from 3 (R-O, O-T, and T-C) to 1 (R-C) around 15% Zr with T_{R-C} = 280 K.[5–7] In addition, a gradual macroscopic crossover from classical

ferroelectric (up to 15% Zr) to an intermediate diffuse regime, and up to a relaxor behavior (above 26% Zr) was observed as the local B-site cationic disorder increases by substituting larger Zr^{4+} (0.72 Å) for Ti^{4+} (0.605 Å). In a different way, substitution of Ca^{2+} (1.34 Å) for Ba^{2+} (1.61 Å) in the large A-site of BT structure is likely to preserve the ferroelectricity as it stabilizes the tetragonal distortion through chemical pressure effect. Indeed, substitution with calcium promotes slight increase of T_{T-C} along with decreases of T_{O-T} and T_{R-O} until they completely disappeared for 23% Ca.[8,9]

Interestingly, investigations of bulk ceramics in the pseudo-binary system $(1-y)BaTi_{0.8}Zr_{0.2}O_3 - yBa_{0.7}Ca_{0.3}TiO_3$ have revealed for y = 0.32 a Phase Convergence Region (PCR) at 340 K, *ie* presence of a quadruple point between R, O, T and C phases.[10,11] Compositions around PCR have demonstrated very large piezoelectric coefficients thanks to the reduction of energy barrier for lattice distortion leading to high flexibility for polarization rotation under moderate external stress.[12,13] These high performances make BCTZ a relevant lead-free alternative to the harmful $PbTi_{1-x}Zr_xO_3$ (PZT) compound for electromechanical technologies.

BCTZ thin films have also been considered to achieve ferroelectric-based tunable devices with attractive properties in comparison with the industrially processed $Ba_{1-x}Sr_xTiO_3$ (BST) compounds.[14–21] Nonetheless, few reports were devoted to the evolution of dielectric properties as a function of temperature and/or frequency over large range of composition.[16,21–24] In particular, none of them evidence an evolution of the dielectric behavior of thin films as it is observed in the complex bulk BCTZ phase diagram. In this context, this report is focused on the exploration of dielectric and tunable properties of $Ba_{1-x}Ca_xTi_{1-x}Zr_xO_3$ ($0 \leq x \leq 0.18$) thin films starting from the well-behave $BaTiO_3$ and increasing the Ca and Zr contents. First, the chemical and structural features of BCTZ thin films obtained through a co-sputtering process are introduced. Second, the attention is focused on the dielectric behavior of thin films as a function of temperature, frequency and electric

field. Finally, the role of composition on the dielectric and tunable performances of thin films are discussed by relying on a systematic comparison with bulk ceramics counterparts (whom experimental results are detailed in Supporting Information) aiming at providing a comprehensive picture of relation between composition and dielectric behavior in the BCTZ system.

2. Experimental Section

BCTZ thin films were deposited by RF magnetron co-sputtering starting with two 3 inch homemade ceramic targets of compositions: $BaTiO_3$ (named hereafter target 1) and $Ba_{0.8}Ca_{0.2}Ti_{0.83}Zr_{0.17}O_3$ targets (named hereafter target 2). Films were deposited on two different substrates: Si(100) and Pt(111)/TiO_x/SiO_2/Si(100) substrates. Prior each deposition, the substrates (20×20 mm²) were thoroughly cleaned in liquid acetone and isopropanol vapor, and subsequently placed in the deposition chamber (Plassys MP700) pumped down to a base pressure of 5.10^{-5} Pa. The depositions were performed in Ar/O_2 plasma (P = 5 Pa, 1% O_2), with the substrate holder at the floating potential, maintained at 650°C and at distance of 10 cm from both ceramic targets. The composition of thin films have been tailored by changing P_{BCTZ} (%) from 0 to 100%, which corresponds to the percent of RF power applied to target 2 according the total power applied on both targets upon deposition.

A first set of thin layers (thicknesses of ~80 nm) were deposited on Si(100) substrates to determine their chemical composition and deposition rate by Rutherford Backscattering Spectroscopy (RBS) and X-Ray Reflectometry (XRR), respectively. RBS analyses were carried out using $4He^+$ ion beams (2 MeV) with a scattering angle of 160°. The spectra were fitted using SIMNRA software. XRR analysis were performed with a Brüker D8 Advance 4-circle diffractometer equipped with a Göbel mirror, using a CuKα1 monochromatic source powered at 40

kV and 40 mA. In view of dielectric measurements, a second set of thicker films were deposited on Pt(111)/TiO_x/SiO_2/Si(100) substrates with thicknesses of 300±10 nm, checked with a dektak 6m Veeco profilometer. The structural characteristics were assessed by X-Ray Diffraction (XRD) analyses, using the same set up as for XRR.

The dielectric characterizations were performed on MIM capacitors, obtained by the deposition of top Pt electrodes (∅ = 600 μm) by magnetron sputtering through a shadow mask over the BCTZ films (300 nm thick). First, the dielectric characteristics (in air and at T_{amb} = 300 K) of all samples were rapidly assessed using a probe station (Karl Süss) to confirm the reproducibility over at least six capacitors. Subsequently, samples were mounted in a home-made cryogenic cell to measure the dielectric properties of selected capacitors as a function of temperature (100 to 420 K) under He atmosphere. In both cases, measurements were conducted by HP A 4194 impedance spectrometer, operating from 100 Hz to 1 MHz with an AC voltage of 0.1 V.

3. Results

The chemical composition of thin films on Si substrates have been determined by Rutherford Backscattering Spectroscopy (RBS). In the hypothesis that all the elements occupied the ABO_3 perovskite structure, atomic ratios of B/A = 1.00 are recorded for all the samples within experimental uncertainties. The atomic ratios Ca/(Ba+Ca) and Zr/(Ti+Zr) are presented in Fig. 1 as a function of P_{BCTZ} (for definition of P_{BCTZ} see section 5. Experimental). It can be noticed that, Ca and mainly Zr contents, are higher than the expected values for a linear evolution of composition from $BaTiO_3$ (target 1) to $Ba_{0.8}Ca_{0.2}Ti_{0.83}Zr_{0.17}O_3$ (target 2) as P_{BCTZ} increases. The compositional deviations between films and targets are hardly interpretable in complex multi-elements system deposited by sputtering techniques. Indeed, it can be attributed to numerous phenomena such as difference of

(re-)sputtering yields, of angular spreads or of re-evaporation between elements. However, it is worth noticing that an over-stoichiometry in zirconium has been reported for sputtered BTZ films and for BCTZ single crystal obtained by Top-Seeded Solution Growth method.[25,26] In the latter case, zirconium over-stoichiometry originates from difference in Zr and Ti effective segregation coefficients. These results suggest that a potential out diffusion of Ti upon BCTZ growth may led to its preferential re-sputtering/evaporation, explaining the abnormally high Zr content in thin films. In the range $0\% \leq P_{BCTZ} \leq 63\%$, a linear increase of Ca and Zr concentrations with P_{BCTZ} is observed, with equal Ca and Zr content in the resolution limit of RBS technique. This equality while the sputtered target includes more Ca than Zr may be ascribed to a preferential segregation of the latter. Hence, in the following of the paper, the attention will be focused on samples obtained with $0 \leq P_{BCTZ} \leq 63\%$ and they will be denominated by the corresponding value x ($0 \leq x \leq 0.18$) in $Ba_{1-x}Ca_xTi_{1-x}Zr_xO_3$ formula. Note that similar compositions for samples obtained with $P_{BCTZ} = 50$ %, deposited at the beginning and at the end of the second set samples, have highlighted the reproducibility of the process.

The structural features of thin films have been systematically analyzed by X-Ray Diffraction (XRD). A representative pattern is presented in Fig. 2. All the samples present a preferentially 111 orientated perovskite structure without secondary phase, in the detection limit of the probing technique. No significant peak shift and peak splitting were observed with the variation of the substitution rate. This effect can be related to chemical fluctuation in BCTZ together with inhomogeneous strain for thin films. All the films were assigned as pseudo-cubic with $a_{pc} = 4.077 \pm 0.005$ Å. Nevertheless, short-range order structure with various symmetries cannot be ruled out in spite of the average pseudo-cubic structure observed by XRD.[27]

The room temperature dielectric properties (ε' and tan δ) of BCTZ thin films are presented in Fig. 3a-b as a function x. The permittivity remains in the range 378-444 for $x \leq 0.12$, while it falls down to 235 when x is further increased up to 0.18. The dielectric losses slowly increase from 1.6% to 2.0% when x varies from 0 to 0.12. Beyond this substitution rate, tan δ decreases down to 1.0% for x = 0.18.

The temperature dependence of the dielectric permittivity for all the compositions (x = 0, 0.04, 0.06, 0.08, 0.10, 0.12, 0.15 and 0.18) and three frequencies (1, 10 and 100 kHz) are presented in Fig. 4a-h. All the samples display only one dielectric anomaly with a maximum in permittivity at a temperature noted T_m, which is attributed to the transition between macroscopic polar to non-polar phases. For low substitution rates (x = 0, 0.04, 0.06 and 0.08), dielectric anomalies are observed on broad temperature ranges, with a gradual reduction of their T_m as the substitution rate increase (from 370 K, 335 K, 325 K to 295 K at 100 kHz, respectively). For all these compositions, the evolutions of the dielectric permittivity with temperature remain frequency independent. For higher substitution rates (x = 0.10, 0.12, 0.15 and 0.18), a continuous decrease of T_m is still observed (from 230 K, 205 K, 172 K to 154 K at 100 kHz, respectively). As a counter-intuitive result, the dielectric anomalies for these substitution rates appear sharper than for the lower ones; in the same time, a more and more pronounced frequency dispersion is observed. These two issues are addressed below.

The broadness of the dielectric anomalies in temperature ($\Delta T_{anomaly}$) is quantified for a frequency of 100 kHz using the following formula:

$$\Delta T_{anomaly} = T_{0.98\varepsilon_m}(above\ T_m) - T_{0.98\varepsilon_m}(below\ T_m) \qquad (1)$$

where $T_{0.98\varepsilon_m}$ values correspond to the temperatures at which 98% of the maximum of permittivity ε_m is measured, below and above T_m. A continuous reduction of $\Delta T_{anomaly}$ is observed when $0 \leq x$

≤ 0.10 (Fig. 5) down to minimum values when the composition reaches the range 0.10 ≤ x ≤ 0.18, highlighting that dielectric anomalies become sharper with the increase of Ca and Zr contents for the range of studied compositions. Nonetheless, in every cases, broad anomalies observed for thin films suggest that local polar region may subsist even above T_m.

For high substitution rates (x = 0.10, 0.12, 0.15 and 0.18), ε'(T) curves reveal a shift of T_m toward higher temperatures as the frequency increases, which is typical to a relaxor behavior. The frequency dispersion (ΔT_m) is characterized using the following formula:

$$\Delta T_m = T_{m(1MHz)} - T_{m(1kHz)} \qquad (2)$$

where $T_{m(1MHz)}$ and $T_{m(1kHz)}$ correspond to T_m at 1 MHz and 1 kHz respectively. In agreement with the classical ferroelectric behavior reported on bulk samples for compositions close to $BaTiO_3$,[4] ΔT_m values remain equal to 0 for 0 ≤ x ≤ 0.08 (Fig. 6). Above this substitution rate, ΔT_m rises with x from 13, 15, 25, to 28 ± 3 K for x = 0.10, 0.12, 0.15 and 0.18, respectively. This evolution underlines the appearance from x = 0.10 and the strengthening of the relaxor behavior with higher Ca/Zr contents.

The tunability of thin films at 100 kHz was calculated using the following formula:

$$tunability\ (\%) = \frac{\varepsilon'_{max} - \varepsilon'_{(E(\varepsilon' max) + E(bias))}}{\varepsilon'_{max}} \times 100 \qquad (3)$$

where ε'_{max} and $\varepsilon'_{(E(\varepsilon' max) + E(bias))}$ (with $E(bias)$ = ± 250 kV.cm^{-1}) were used to take into consideration the slight shift of $\varepsilon'(E)$ curves ($E(\varepsilon' max) \neq 0$ kV.cm^{-1}) due to some asymmetric behaviors at bottom and top electrodes/BCTZ interfaces. Fig. 7 presents, for each BCTZ film, the tunabilities measured at room temperature (300 K) and at its T_m. At room temperature, the tunability remarkably presents a non-monotonous evolution with x. It is improved from 25% to 40% when x varies from 0 to 0.12, and rapidly decreases down to 15% when x is further increased. This peculiar

trend is even enhanced for tunability measured at T_m. As an example, a maximum of 49% is obtained for x = 0.12 when its tunability is measured at its T_m = 205 K.

4. Discussion

In order to get a deeper insight in the evolution of the dielectric behavior with composition, a comparison between BCTZ thin films and bulk ceramic counterparts is presented. The transition temperatures for bulk ceramics (T_{R-O}, T_{O-T} and T_{T-C} or T_{R-C} where applicable) and for thin films (T_m) are plotted in Fig. 8 as a function of x along with the corresponding classical ferroelectric, diffuse or relaxor behavior. Note that the dielectric measurements of ceramic samples are presented in Fig. S1 in Supporting Information.

For bulk samples, three transitions (R-O, O-T and T-C) are detectable for $0 \leq x \leq 0.12$. The transition temperatures (T_{R-O}, T_{O-T} and T_{T-C}) are far from each other for x = 0 and tend to come together in the PCR as x increases up to 0.12. For $0.15 \leq x \leq 0.18$, the transition R-C is solely detected. The dielectric behavior changes from classical ferroelectric ($0 \leq x \leq 0.12$), to an intermediate diffuse behavior (x = 0.15), and finally to relaxor regime (x = 0.18), in agreement with the published data. [4] The transition temperatures between low temperature polar phase to high temperature non-polar phase are noted T_M, both for T_{T-C} ($0 \leq x \leq 0.12$) and for T_{R-C} ($0.15 \leq x \leq 0.18$). On the whole composition range, a continuous decrease of T_M with increasing x is observed. For thin films, only one broad anomaly is detected in all the ε'(T) curves (Fig. 4a-h). The maxima in ε', at the temperatures noted T_m, correspond to the transition between macroscopic low temperature polar phase to high temperature non-polar phase. As for bulk ceramics, a monotonous decrease of T_m with x is observed. Nevertheless, T_m values are downshifted in comparison with T_M values

considering equivalent compositions. In addition, the relaxor regime is observed for substitution rate as low as x = 0.10 for thin films, while it is observed for x = 0.18 in the case of bulk ceramics.

The macroscopic relaxor behavior for BCTZ is ascribed to the formation of polar nano-clusters (Ti-rich ordered regions) in a less-polar host (containing disordered Ti and Zr).[28,29] The elementary units that lead to the observed dielectric properties are thus assigned to local electric dipoles resulting from the correlated off-centering of Ti^{4+} within clusters of temperature dependent sizes. Chemical heterogeneity and lower polarizability of Zr as compared to Ti are the main ingredients for this model. For both bulk and thin film specimens, continuous crossover from classical ferroelectric to relaxor behavior along with a decrease of T_M and T_m are directly linked to the increase of Zr content in a disordered B-site cationic network in the case of BCTZ solid-solution. It is worth noticing that the decrease of T_M in BCTZ is moderated by the presence of small Ca^{2+} in the A-site cationic network, in comparison with similar Zr contents in the Ca-free $BaTi_xZ_{1-x}O_3$ system.[5–7] The discrepancies between films and ceramics are related to extrinsic contributions for thin layers such as reduction of grain size below polar domain size, inhomogeneous residual stress, higher compositional fluctuations, interface contributions.[30–35] These effects promote higher dispersion of polar-region size and correlation length that lead, ultimately, to a broadening of temperature-induced transitions along with a reduction of the stability for macroscopic polar phases versus temperature ($T_M > T_m$). Consequently, the broad anomalies in ε'(T) curves for $0 \leq x \leq 0.08$ (see large values for $\Delta T_{anomalie}$ in Fig. 5) can result from the overlap of the three expected dielectric anomalies for such compositions (for the sequences R-O, O-T and T-C). Furthermore, the sharper anomalies when $0.10 \leq x \leq 0.18$ (see reduction of $\Delta T_{anomalie}$ in Fig. 5) reflect that these compositions meet a PCR similarly to bulk counterparts, with transition temperatures downshifted of about 100 K for thin films. Remarkably, these results show that the convergence of transition

temperatures is determined by the chemical composition in BCTZ system (PCR around x = 0.12 for $Ba_{1-x}Ca_xTi_{1-x}Zr_xO_3$ whatever the processing condition for sample preparation) and that the temperature of convergence can be adjusted by microstructural contributions (grain size, strain…), as highlighted by the extended PCR represented by a grey rectangle in Fig. 8.

The highest tunability is obtained for thin films with x = 0.12, a composition close to PCR (Fig. 7). It is worth recalling that this composition is equivalent to y = 0.4 in the pseudo-binary $(1-y)BaTi_{0.8}Zr_{0.2}O_3 - yBa_{0.7}Ca_{0.3}TiO_3$ system and has displayed among the highest piezoelectric response for BCTZ bulk ceramics.[12] Therefore, the high tunability can be partially explained by an enhanced polarization flexibility to moderate external stresses (either pressure or electric field) thanks to a reduction of the difference of free energy between the polar phases in competition at the vicinity of PCR.[12,13,36] Coexistence of the different polar phases and the instability of the polarization orientations have also been reported to play a major role in the enhancement of the tunability in other systems.[37] On the other hand, the tunability should reach a maximum close to the ferroelectric-to-paralelectric transition temperature, named Curie temperature T_C for a classical ferroelectric (named in this work T_m or T_M for thin film and bulk ceramic samples, respectively, to take into consideration that the dielectric behavior varies from classical ferroelectric to relaxor regime).[38,39] This is experimentally evidenced by comparing the two curves in Fig. 7 and in other systems like the well-known $Ba_{1-x}Sr_xTiO_3$, for which T_C can be tailored by A-site substitution without breaking down the classical ferroelectric behavior.[1] Thus, in the present study, it can be surprising that the highest room temperature tunability is not obtained for thin films with x = 0.06 (T_m = 295 K) but for thin films with x = 0.12 (T_m = 205 K). These results suggest that the local chemical disorder in BCTZ system still play a major macroscopic contribution, even far above T_m. As mentioned earlier, the increase of Ca and Zr contents leads to a crossover from classical

ferroelectric to relaxor behavior due to a more disordered cationic arrangement. In complex perovskite system, this effect is generally accompanied with an increase of the diffuse character of the temperature-induced transitions. The diffuseness of the transitions at 100 kHz can be assessed through the determination of the critical parameters γ in a modified Curie-Weis law:[40,41]

$$\frac{1}{\varepsilon'} - \frac{1}{\varepsilon'_m} = \frac{(T-T_m)^\gamma}{C} \qquad (4)$$

where C and γ are constant values extracted from the linear fits of $Ln(\frac{1}{\varepsilon'} - \frac{1}{\varepsilon'_m})$ versus $Ln(T - T_m)$ plots in the paraelectric regime above T_m in the range +30 to +55 K (Fig. S2). Since the onset of permanent dipoles in an ideal ferroelectric follows the classical Curie-Weiss law, the critical parameter γ provides some information on the deviation to long-range ordered system. It varies from γ = 1 for classical ferroelectric phase transition to γ = 2 for diffuse phase transition with highly disordered configuration. For bulk ceramics, a monotonous variation of γ from 1.0 to 1.9 is observed as x is raised from 0 to 0.18 (Fig. 9), in line with the continuous crossover from ferroelectric to relaxor. Astonishingly, the evolution of γ for thin film samples displays a different trend. The critical parameter rises from γ = 1.42 for x = 0 to a maximum value of γ = 1.99 for x = 0.12. Beyond this substitution rate, a decrease of γ is observed despite a strengthening of the relaxor behavior (see increase of ΔT_m in Fig. 6). The higher values of γ for thin films compared to ceramics can be mainly traced back, as discussed before, to discrepancies in (micro)structural features leading to higher concentrations of defects for sputtered layers.[30–35] Note that similar trends have been reported for BCTZ ceramics densified by conventional sintering and spark plasma sintering processes.[42] The highest value of γ for BCTZ thin films with x = 0.12 results from a highly disordered system due to the competition between long range and short range order. This configuration is promoted by the presence of polar clusters having various correlation length in a non-polar host, which is evidenced by an emerging relaxor behavior for these Ca and Zr contents. In addition, the local

disorder may be strengthened with the coexistence of T, O and R polar phases due to the vicinity of the PCR for x = 0.12. Regarding the latter point, structural instabilities around PCR should provide an easier accommodation of residual stress for thin films through phase transitions upon cooling. Such relaxation process may lead to a higher distribution of polar cluster of different phases along with a reduction of their size responsible for an increase of γ parameter. This issue deserves further characterizations addressed in future works.

In summary, the improved tunability for BCTZ thin films with x = 0.12 can be explained by the concomitance of two phenomena (note that a summary of the collected dielectric data on thin films is presented in Table S1). First, the highest non-linear dependence of dielectric permittivity to electric field originates from an optimized number and size of polar-cluster in the non-polar matrix. As evidenced on other systems,[38,39] the best properties arise from the best compromise between high concentrations of polar clusters but sufficiently diluted in the non-polar host to enable their extension under moderate external electric field. This is evidenced for films with x = 0.12 by an emerging relaxor behavior (see ΔT_m in Fig. 6) in highly disordered configuration (see the highest γ of 1.99 in Fig. 9) together with a dielectric permittivity remaining high (see ε' = 443 in Fig. 3). Second, the presence of structural flexibility due to degeneracy of T, O and R polar phases around the PCR for films with x = 0.12 further improve the dielectric properties (see the low $\Delta T_{anomaly}$ in Fig. 5). This configuration may promotes a high distribution of phases in polar clusters even far above T_m along with their easy extension upon poling due to instability of the polarization orientations in the vicinity of the PCR.[43]

5. Conclusions

The dielectric properties of $Ba_{1-x}Ca_xTi_{1-x}Zr_xO_3$ thin films and bulk ceramics ($0 \leq x \leq 0.18$) are presented as a function of temperature and frequency. In both cases, the following features are observed: i) a gradual crossover from classical ferroelectric-to-relaxor behavior together with a decrease of the transition temperature between macroscopic polar to non-polar phases as the compositions vary from $BaTiO_3$ down to $BaZrO_3$-$CaTiO_3$; ii) a phase convergence region (PCR) for x close to 0.12.

The room temperature tunability of thin films present an optimal value of 40% for the same composition x = 0.12, despite its transition temperature is as low as 205 K. This shows that this composition range which leads to exceptional piezoelectric properties is also the most non-linear even far from the transition temperature. These unusual features are ascribed to an optimized number and size of polar clusters resulting from an emerging relaxor behavior for these Ca and Zr contents along with their easy coarsening due to the vicinity of the PCR.

As a whole, comparison between thin films and ceramics highlights that the occurrence of PCR is intrinsically governed by the chemical composition of BCTZ (with x close to 0.12 in $Ba_{1-x}Ca_xTi_{1-x}Zr_xO_3$) and the temperature of convergence can be shifted by extrinsic contributions (grain size, strain) within an extended PCR. These results pave the way to further improvements for BCTZ functional performances through tailoring of their microstructural properties.

Acknowledgements

This work has been supported by the French government and STMicroelectronics through the project Investissement d'Avenir Tours2015. The authors would like to thank Stéphanie Sorieul

for her fruitful support for RBS characterizations and Kévin Gille for his support for the synthesis of bulk ceramics.

References

[1] A.K. Tagantsev, V.O. Sherman, K.F. Astafiev, J. Venkatesh, N. Setter, Ferroelectric Materials for Microwave Tunable Applications, J. Electroceramics. 11 (2003) 5–66.

[2] S. Gevorgian, Ferroelectrics in Microwaves Devices, Circuits and Systems, Springer, 2009.

[3] G. Subramanyam, M.W. Cole, N.X. Sun, T.S. Kalkur, N.M. Sbrockey, G.S. Tompa, X. Guo, C. Chen, S.P. Alpay, G.A.R. Jr., K. Dayal, L.-Q. Chen, D.G. Schlom, Challenges and opportunities for multi-functional oxide thin films for voltage tunable radio frequency/microwave components, J. Appl. Phys. 114 (2013) 191301. doi:10.1063/1.4827019.

[4] J. Ravez, C. Broustera, A. Simon, Lead-free ferroelectric relaxor ceramics in the BaTiO3-BaZrO3-CaTiO3 system, J. Mater. Chem. 9 (1999) 1609–1613. doi:10.1039/a902335f.

[5] D. Hennings, A. Schnell, G. Simon, Diffuse Ferroelectric Phase Transitions in Ba(Ti1-yZry)O3 Ceramics, J. Am. Ceram. Soc. 65 (1982) 539–544. doi:10.1111/j.1151-2916.1982.tb10778.x.

[6] T. Maiti, R. Guo, A.S. Bhalla, Structure-Property Phase Diagram of BaZrxTi1−xO3 System, J. Am. Ceram. Soc. 91 (2008) 1769–1780. doi:10.1111/j.1551-2916.2008.02442.x.

[7] A.K. Kalyani, A. Senyshyn, R. Ranjan, Polymorphic phase boundaries and enhanced piezoelectric response in extended composition range in the lead free ferroelectric BaTi1−xZrxO3, J. Appl. Phys. 114 (2013) 14102. doi:10.1063/1.4812472.

[8] T. Mitsui, W.B. Westphal, Dielectric and X-Ray Studies of CaxBa1-xTiO3 and CaxSr1-

xTiO3, Phys. Rev. 124 (1961) 1354–1359. https://link.aps.org/doi/10.1103/PhysRev.124.1354.

[9] D. Fu, M. Itoh, S. Koshihara, T. Kosugi, S. Tsuneyuki, Anomalous Phase Diagram of Ferroelectric (Ba,Ca)TiO3 Single Crystals with Giant Electromechanical Response, Phys. Rev. Lett. 100 (2008) 227601. https://link.aps.org/doi/10.1103/PhysRevLett.100.227601.

[10] D.S. Keeble, F. Benabdallah, P.A. Thomas, M. Maglione, J. Kreisel, Revised structural phase diagram of (Ba0.7Ca0.3TiO3)-(BaZr0.2Ti0.8O3), Appl. Phys. Lett. 102 (2013) 92903. doi:10.1063/1.4793400.

[11] D. Xue, J. Gao, Y. Zhou, X. Ding, J. Sun, T. Lookman, X. Ren, Phase transitions and phase diagram of Ba(Zr0.2Ti0.8)O3-x(Ba0.7Ca0.3)TiO3 Pb-free system by anelastic measurement, J. Appl. Phys. 117 (2015) 124107. doi:10.1063/1.4916713.

[12] W. Liu, X. Ren, Large Piezoelectric Effect in Pb-Free Ceramics, Phys. Rev. Lett. 103 (2009) 257602. https://link.aps.org/doi/10.1103/PhysRevLett.103.257602.

[13] T. Yang, X. Ke, Y. Wang, Mechanisms Responsible for the Large Piezoelectricity at the Tetragonal-Orthorhombic Phase Boundary of (1-x)BaZr0.2Ti0.8O3-xBa0.7Ca0.3TiO3 System, Sci. Rep. 6 (2016) 33392. doi:10.1038/srep33392.

[14] T.S. Kalkur, W.C. Yi, Dielectric and Tunable Properties of Ba0.96Ca0.04Ti0.84Zr0.16O3 (BCTZ) on MgO and SiO2/Si Substrates, Integr. Ferroelectr. 45 (2002) 123–129. doi:10.1080/10584580215365.

[15] N. Cramer, E. Philofsky, L. Kammerdiner, T.S. Kalkur, Low temperature deposited Ba0.96Ca0.04Ti0.84Zr0.16O3 thin films on Pt electrodes by radio frequency magnetron sputtering, Appl. Phys. Lett. 84 (2004) 771–773. doi:10.1063/1.1645313.

[16] C. Bhardwaj, D. Kaur, Relaxor characteristics of highly tunable lead-free

0.5Ba(Zr0.2Ti0.8)O3-0.5(Ba0.7Ca0.3)TiO3 thin film grown on LaNiO3/Si by pulsed laser deposition, Curr. Appl. Phys. 12 (2012) 1239–1243. doi:http://dx.doi.org/10.1016/j.cap.2012.02.046.

[17] Z. Feng, N. Wu, W. Zhang, J. Luo, X. Tang, Z. Cheng, D. Shi, S. Dou, High dielectric tunability of Ba(Zr0.2Ti0.8)O3–(Ba0.7Ca0.3)TiO3 thick films modified by a solution-immersion process, Mater. Res. Bull. 76 (2016) 384–388. doi:http://dx.doi.org/10.1016/j.materresbull.2016.01.008.

[18] Y. Lin, G. Wu, N. Qin, D. Bao, Structure, dielectric, ferroelectric, and optical properties of (1−x)Ba(Zr0.2Ti0.8)O3−x(Ba0.7Ca0.3)TiO3 thin films prepared by sol–gel method, Thin Solid Films. 520 (2012) 2800–2804. doi:http://dx.doi.org/10.1016/j.tsf.2011.12.030.

[19] W. Li, J. Hao, H. Zeng, J. Zhai, Dielectric and piezoelectric properties of the Ba0.92Ca0.08Ti0.95Zr0.05O3 thin films grown on different substrate, Curr. Appl. Phys. 13 (2013) 1205–1208. doi:http://dx.doi.org/10.1016/j.cap.2013.03.015.

[20] P. Venkata Sreenivas, K.P. Dhiren, A. Shiva, R. Martínez, S. Punam, J.F. Scott, C. V Ramana, B.C. Douglas, S.K. Ram, Nanoscale polarisation switching and leakage currents in (Ba0.955Ca0.045)(Zr0.17Ti0.83)O3 epitaxial thin films, J. Phys. D. Appl. Phys. 48 (2015) 355502. http://stacks.iop.org/0022-3727/48/i=35/a=355502.

[21] C.J.M. Daumont, Q. Simon, E. Le Mouellic, S. Payan, P. Gardes, P. Poveda, B. Negulescu, M. Maglione, J. Wolfman, Tunability, dielectric, and piezoelectric properties of Ba(1−x)CaxTi(1−y)ZryO3 ferroelectric thin films, J. Appl. Phys. 119 (2016) 94107. doi:10.1063/1.4942924.

[22] Y. Lin, N. Qin, G. Wu, T. Sa, D. Bao, Dielectric relaxor behaviors and tunability of (1−x)Ba(Zr0.2Ti0.8)O3–x(Ba0.7Ca0.3)TiO3 thin films fabricated by sol–gel method, Appl.

Phys. A. 109 (2012) 743–749. doi:10.1007/s00339-012-7110-4.

[23] F. Kurokawa, A. Mori, Y. Tsujiura, H. Hida, I. Kanno, Compositional dependence of Ba(Zr0.2Ti0.8)O3–(Ba0.7Ca0.3)TiO3 piezoelectric thin films prepared by combinatorial sputtering, Thin Solid Films. 588 (2015) 34–38. doi:http://dx.doi.org/10.1016/j.tsf.2015.04.050.

[24] L. Huang, Y. Dai, Y. Wu, X. Pei, W. Chen, Enhanced ferroelectric and piezoelectric properties of (1-x)BaZr0.2Ti0.8O3–xBa0.7Ca0.3TiO3 thin films by sol–gel process, Appl. Surf. Sci. 388 (2016) 35–39. doi:http://dx.doi.org/10.1016/j.apsusc.2016.05.030.

[25] V. Reymond, S. Payan, D. Michau, J.-P. Manaud, M. Maglione, Structural and electrical properties of BaTi1−xZrxO3 sputtered thin films: effect of the sputtering conditions, Thin Solid Films. 467 (2004) 54–58. doi:http://dx.doi.org/10.1016/j.tsf.2004.03.005.

[26] F. Benabdallah, P. Veber, M. Prakasam, O. Viraphong, K. Shimamura, M. Maglione, Continuous cross-over from ferroelectric to relaxor state and piezoelectric properties of BaTiO3-BaZrO3-CaTiO3 single crystals, J. Appl. Phys. 115 (2014) 144102. doi:10.1063/1.4870933.

[27] V.R. Mastelaro, H.R. Favarim, A. Mesquita, A. Michalowicz, J. Moscovici, J.A. Eiras, Local structure and hybridization states in Ba0.9Ca0.1Ti1−xZrxO3 ceramic compounds: Correlation with a normal or relaxor ferroelectric character, Acta Mater. 84 (2015) 164–171. doi:https://doi.org/10.1016/j.actamat.2014.10.059.

[28] A. Simon, J. Ravez, M. Maglione, The crossover from a ferroelectric to a relaxor state in lead-free solid solutions, J. Phys. Condens. Matter. 16 (2004) 963. http://stacks.iop.org/0953-8984/16/i=6/a=023.

[29] V. Buscaglia, S. Tripathi, V. Petkov, M. Dapiaggi, M. Deluca, A. Gajović, Y. Ren, Average

and local atomic-scale structure in BaZr x Ti 1− x O 3 (x = 0.10, 0.20, 0.40) ceramics by high-energy x-ray diffraction and Raman spectroscopy, J. Phys. Condens. Matter. 26 (2014) 65901. http://stacks.iop.org/0953-8984/26/i=6/a=065901.

[30] C.M. Carlson, T. V Rivkin, P.A. Parilla, J.D. Perkins, D.S. Ginley, A.B. Kozyrev, V.N. Oshadchy, A.S. Pavlov, Large dielectric constant (ε/ε0>6000)Ba0.4Sr0.6TiO3 thin films for high-performance microwave phase shifters, Appl. Phys. Lett. 76 (2000) 1920–1922. doi:10.1063/1.126212.

[31] C.B. Parker, J.P. Maria, A.I. Kingon, Temperature and thickness dependent permittivity of (Ba,Sr)TiO3 thin films, Appl. Phys. Lett. 81 (2002) 340–342. http://link.aip.org/link/?APL/81/340/1.

[32] S. Tong, M. Narayanan, B. Ma, R.E. Koritala, S. Liu, U. Balachandran, D. Shi, Effect of dead layer and strain on the diffuse phase transition of PLZT relaxor thin films, Acta Mater. 59 (2011) 1309–1316. doi:http://dx.doi.org/10.1016/j.actamat.2010.10.063.

[33] W.K. Simon, E.K. Akdogan, A. Safari, J. Bellotti, Effect of misfit strains on fourth and sixth order permittivity in (Ba0.60Sr 0.40)TiO3 films on orthorhombic substrates, Appl. Phys. Lett. 88 (2006) 132902–132903. http://link.aip.org/link/?APL/88/132902/1.

[34] R.P.S.M. Lobo, N.D.S. Mohallem, R.L. Moreira, Grain-Size Effects on Diffuse Phase Transitions of Sol-Gel Prepared Barium Titanate Ceramics, J. Am. Ceram. Soc. 78 (1995) 1343–1346. doi:10.1111/j.1151-2916.1995.tb08492.x.

[35] J. Hao, W. Bai, W. Li, J. Zhai, Correlation Between the Microstructure and Electrical Properties in High-Performance (Ba0.85Ca0.15)(Zr0.1Ti0.9)O3 Lead-Free Piezoelectric Ceramics, J. Am. Ceram. Soc. 95 (2012) 1998–2006. doi:10.1111/j.1551-2916.2012.05146.x.

[36] A.G. Khachaturyan, Ferroelectric solid solutions with morphotropic boundary: Rotational instability of polarization, metastable coexistence of phases and nanodomain adaptive states, Philos. Mag. 90 (2010) 37–60. doi:10.1080/14786430903074789.

[37] P. Li, W. Li, J. Zhai, B. Shen, H. Zeng, K. Zhao, Composition dependence of phase structure and electrical properties of BiMnO3-modified Bi0.5(Na0.8K0.2)0.5TiO3 thin films, RSC Adv. 5 (2015) 62713–62718. doi:10.1039/C5RA10795D.

[38] M. Maglione, M.L. Dos Santos, M.R. Chaves, A. Almeida, Critical Exponents and Randomness in SrTiO3 : Ca, Phys. Status Solidi. 181 (1994) 73–80. doi:10.1002/pssb.2221810108.

[39] O. Bidault, M. Maglione, Non-Linearity Extremum in Niobium Doped Potassium Tantalate, J. Phys. I Fr. 7 (1997) 543–552. https://doi.org/10.1051/jp1:1997106.

[40] K. Uchino, S. Nomura, Critical exponents of the dielectric constants in diffused-phase-transition crystals, Ferroelectrics. 44 (1982) 55–61. doi:10.1080/00150198208260644.

[41] A.A. Bokov, Z.G. Ye, Phenomenological description of dielectric permittivity peak in relaxor ferroelectrics, Solid State Commun. 116 (2000) 105–108. doi:http://dx.doi.org/10.1016/S0038-1098(00)00295-7.

[42] F. Benabdallah, C. Elissalde, U.-C.C. Seu, D. Michau, A. Poulon-Quintin, M. Gayot, P. Garreta, H. Khemakhem, M. Maglione, Structure–microstructure–property relationships in lead-free BCTZ piezoceramics processed by conventional sintering and spark plasma sintering, J. Eur. Ceram. Soc. 35 (2015) 4153–4161. doi:http://dx.doi.org/10.1016/j.jeurceramsoc.2015.06.030.

[43] N.D. Scarisoreanu, F. Craciun, A. Moldovan, V. Ion, R. Birjega, C. Ghica, R.F. Negrea, M. Dinescu, High Permittivity (1 – x)Ba(Zr0.2Ti0.8)O3 – x(Ba0.7Ca0.3)TiO3 (x = 0.45)

Epitaxial Thin Films with Nanoscale Phase Fluctuations, ACS Appl. Mater. Interfaces. 7 (2015) 23984–23992. doi:10.1021/acsami.5b06745.

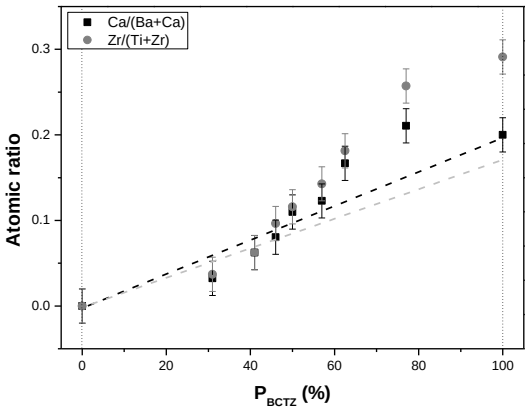

Fig. 1. Atomic ratios Ca/(Ba+Ca) and Zr/(Ti+Zr) as a function of P_{BCTZ} extracted from RBS measurements. Dashed lines correspond to linear ratios vs P_{BCTZ}.

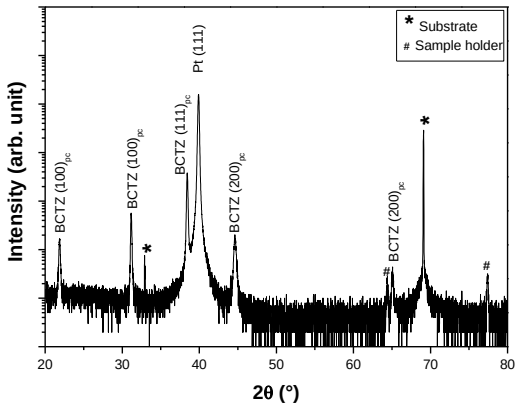

Fig. 2. Representative XRD pattern of a BCTZ thin films on Pt(111)/TiO_x/SiO_2/Si(100) substrate. Peaks are indexed in the pseudo-cubic perovskite structure.

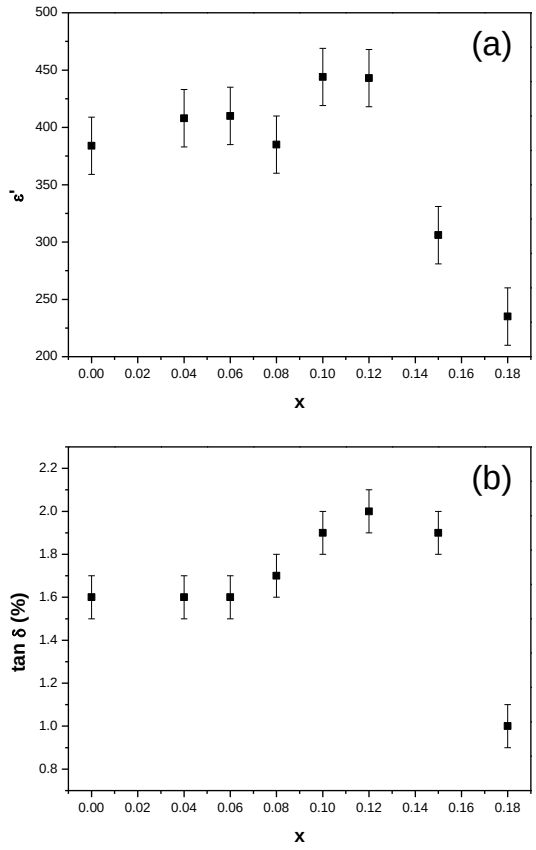

Fig. 3. Dependence of ε' (a) and tan δ (b) for $Ba_{1-x}Ca_xTi_{1-x}Zr_xO_3$ thin films, at room temperature and 100 kHz, as a function x.

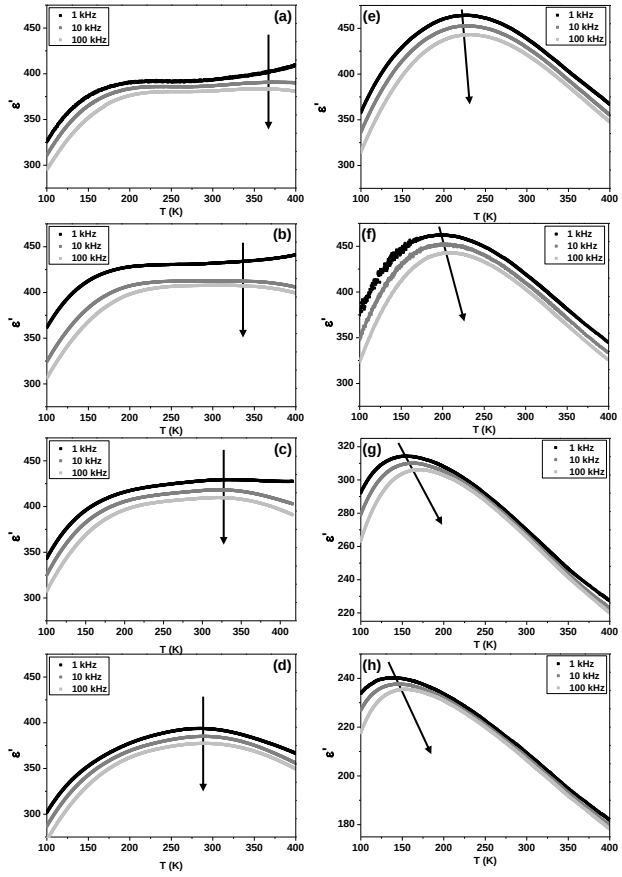

Fig. 4. Temperature dependence of ε' as a function of temperature for $Ba_{1-x}Ca_xTi_{1-x}Zr_xO_3$ thin films with x = 0 (a), 0.04 (b), 0.06 (c), 0.08 (d), 0.10 (e), 0.12 (f), 0.15 (g), and 0.18 (h). Arrows are guides for the eyes to highlight the evolution of T_m with the three measurement frequencies (1 kHz, 10 kHz, 100 kHz).

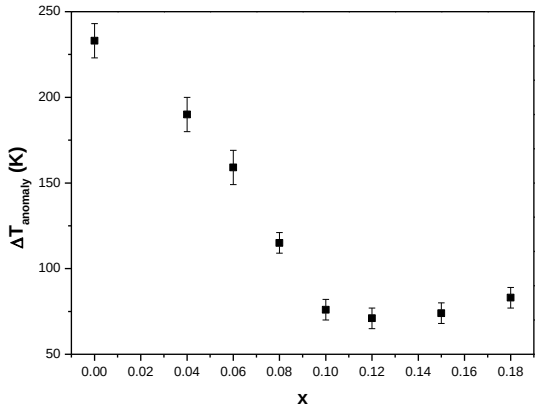

Fig. 5. Evolution of $\Delta T_{anomaly}$ at 100 kHz for $Ba_{1-x}Ca_xTi_{1-x}Zr_xO_3$ thin films as a function of x.

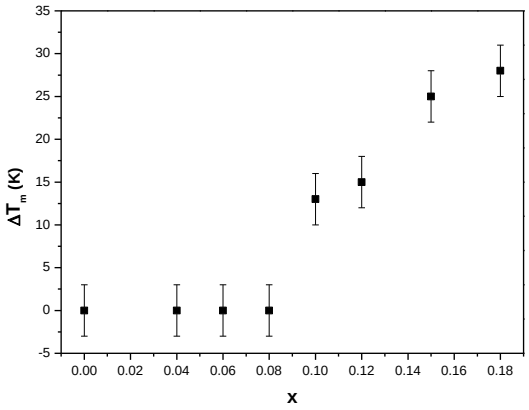

Fig. 6. Evolution of ΔT_m for $Ba_{1-x}Ca_xTi_{1-x}Zr_xO_3$ thin films as a function of x.

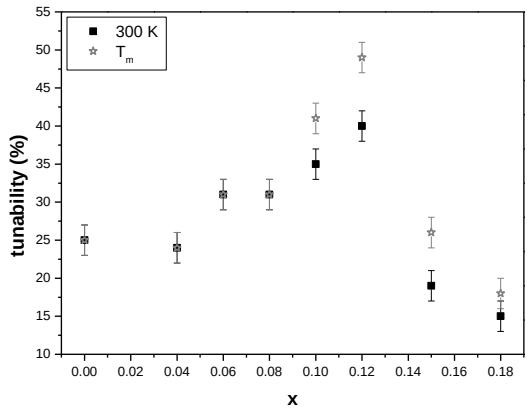

Fig. 7. Tunability (%) at 100 kHz for $Ba_{1-x}Ca_xTi_{1-x}Zr_xO_3$ thin films as a function of x, measured at room temperature and at T_m.

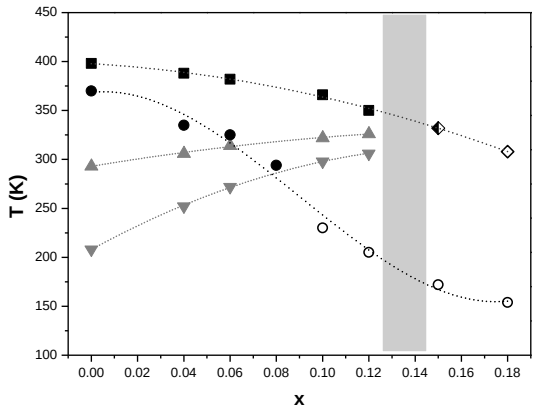

Fig. 8. Phase diagram of $Ba_{1-x}Ca_xTi_{1-x}Zr_xO_3$ thin films and bulk ceramics deduced from dielectric measurements at 100 kHz. For bulk ceramics, the symbols ■, ▲ and ▼ correspond to T_{T-C} T_{O-T}, T_{R-O}, respectively, when $0 \leq x \leq 0.12$, while ♦ represent the T_{R-C} when $0.15 \leq x \leq 0.18$. For thin film, symbols ● report the Tm. In both cases, filled, half-filled and open symbols correspond to classical ferroelectric, intermediate diffuse regime, and relaxor behavior, respectively. The extended Phase Convergence Region (PCR) is represented by a grey rectangle. Dashed lines are guides for the eyes.

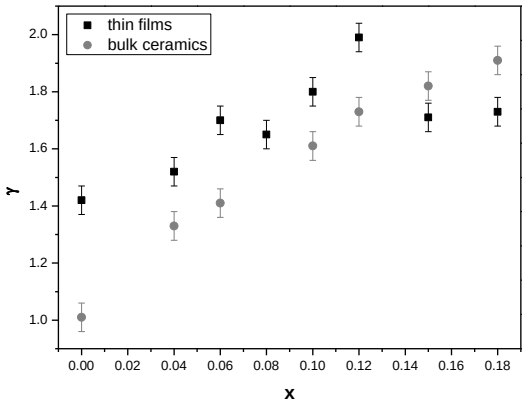

Fig. 9. Evolution of critical exponent γ for $Ba_{1-x}Ca_xTi_{1-x}Zr_xO_3$ thin films and bulk ceramics as a function of x, extracted from modified Curie-Weiss law fits.